

Hidden-Field Coordination Reveals Payoff-Free Quantum Correlation Structure in Decentralized Coordination

Sinan Bugu^{1, 2, *}

¹Department of Physics and Astronomy, North Carolina State University, Raleigh, North Carolina, USA

²BuQuLab Research Laboratory, Winston-Salem, North Carolina, USA

(Dated: January 30, 2026)

We study decentralized multi-agent coordination where agents must correlate actions against an unobserved field and cannot communicate. To isolate correlation geometry from payoff optimization, we introduce the Hidden-Field Coordination (HFC) model, which enforces identical information access and no-signaling constraints across strategies. Using information-theoretic diagnostics, we compare classical shared-randomness baselines with an entanglement-mediated strategy based on multipartite W states and a strictly local *Spontaneous Leader Election* rule. Within the restricted symmetric shared-latent baseline studied here, increasing total correlation is achieved primarily by driving actions toward alignment (copying), which also increases pairwise coincidence (collisions). By contrast, the quantum strategy realizes a collision-suppressing coordination regime: it preserves global dependence while reducing pairwise coincidence below the independent (product) baseline induced by the common marginal distribution. This produces a geometric separation in the joint-action distribution. Classical baselines concentrate probability near the diagonal of action equality, whereas the entanglement-mediated mapping occupies an offset-diagonal region associated with relational roles. Accordingly, the entanglement signature in this setting is not higher correlation magnitude; total-correlation differentials can be negative relative to the classical copying optimum. Instead, it reflects a change in dependence geometry that supports robust anti-coordination.

I. INTRODUCTION

Decentralized multi-agent systems often exhibit coordination patterns that cannot be inferred from any single agent’s local rule. In many practical settings, agents cannot communicate, the coordination channel is constrained, and the environment imposes latent, round-by-round randomness that reshapes which joint actions are favorable or penalized. In such settings, the central scientific question is not whether a mechanism “wins,” but what *correlation structure* it induces in the empirical joint-action distribution under identical external constraints.

A fundamental tension exists in the *restricted* classical coordination family we study here: when agents are constrained to use a symmetric shared-latent mechanism that correlates actions primarily by increasing action-equality (copying), stronger statistical dependence typically coincides with higher collision probability. In the limit of maximal correlation within this shared-latent family, agents achieve perfect dependence by outputting identical actions. While this maximizes information-theoretic metrics like total correlation, it is catastrophic for tasks requiring distributed coverage, load balancing, or anti-coordination, where local action collisions are penalized. Throughout, claims about an “alignment trade-off” refer to this explicit classical baseline family (defined in Sec. II) rather than to arbitrary classical shared-randomness strategies.

Quantum platforms provide a distinctive route to

break this trade-off. Multipartite entanglement can generate non-product joint statistics that sustain global dependence without forcing local alignment. In this work, we implement this via a *Spontaneous Leader Election* protocol. Unlike idealized models that assume global knowledge of all measurement outcomes to resolve ties, our agents act solely on local measurement results. This ensures that the coordination is strictly decentralized and respects the no-signaling constraints of relativistic physics. Such possibilities are discussed in the broader context of nonclassical correlations and nonlocality [1–10].

Assessing multipartite correlation structure in realistic, noisy settings benefits from observables that are explicitly distributional. Information-theoretic functionals provide a natural language for this purpose [11–16]. However, payoff-driven framings can obscure a simpler, more transferable object: the *geometry of correlations* in the joint-action distribution. Specifically, does the coordination mechanism force agents onto a “diagonal” of identical actions, or does it allow them to occupy collision-suppressing regions of the probability space? [17–23].

Here we introduce the *Hidden-Field Coordination* (HFC) model as a minimal framework designed to isolate this geometric distinction. In HFC, each round begins with an exogenous latent “field” that remains unobserved by agents. This construction enforces a strict separation between the externally imposed latent structure and the coordination mechanism among agents. A classical shared-latent baseline provides a controlled common-cause model of correlation, while an entanglement-mediated strategy provides a nonclassical correlated sampling mechanism. Crucially, the quantum-to-action mapping is fixed and index-equivariant, ensur-

* sbugu@ncsu.edu; sinanbugu@gmail.com

ing that observed differences reflect distributional structure rather than tailored utility exploitation. Figure 1 schematically summarizes the HFC generative process.

We characterize coordination using the *average pairwise mutual information* (APMI) and the *total correlation* (TC) [11–14]. To isolate the geometric separation between strategies, we report *differentials* relative to the strongest classical baseline. As shown in our results, a negative differential in these metrics indicates that the quantum strategy has sacrificed raw correlation magnitude—the “alignment trap”—to achieve a collision-suppressing geometry. This perspective aligns with recent views of coordination and shared randomness as resources in multi-agent quantum settings [24].

We implement the entanglement-mediated strategy using W states, which are natural candidates for distributed coordination because they retain entanglement under single-particle loss [25–34]. Our focus is therefore a minimal model of multipartite coordination under realistic NISQ-era constraints [35–38].

The remainder of the paper is organized as follows. Section II defines the HFC generative process and the local leader election rule. Section III presents numerical results and the associated correlation-structure diagnostics. Section IV describes the simulation pipeline and metrics.

II. HIDDEN-FIELD COORDINATION MODEL

We introduce the Hidden-Field Coordination (HFC) model as a minimal probabilistic framework for analyzing correlation structure in decentralized multi-agent systems under partial information. The defining feature of the model is an exogenous, round-by-round random latent variable that reshapes which joint action patterns are penalized or favored, without being directly observable by the agents. The model is deliberately constructed to separate correlation structure from payoff optimization, communication, or equilibrium reasoning.

A. Generative structure

Consider N agents, each selecting an action from a finite alphabet $\mathcal{A} = \{1, \dots, M\}$. Each round proceeds according to the following generative process.

At the start of the round, a hidden field F is sampled from a fixed distribution. In the instantiations studied here, F corresponds to a random selection of K unfavorable targets among the M available actions. The field is exogenous, fixed throughout the round, and inaccessible to all agents.

Each agent i produces an initial action proposal $\tilde{a}_i \in \mathcal{A}$ according to a strategy-dependent sampling rule. Agents do not communicate, do not observe each other’s actions, and do not observe F . Any correlation between agents

must therefore arise from shared resources established prior to the round.

A local “intel” process then perturbs each agent’s proposed action independently with probability $p \in [0, 1]$. The intel process is memoryless and depends only on the agent’s current proposal and its noisy local interaction with the hidden field, with no dependence on past rounds or other agents. After this perturbation, each agent outputs a final action a_i . No utility function or equilibrium concept is invoked; the analysis focuses purely on the resulting empirical joint-action distribution $P(a_1, \dots, a_N)$.

B. Strategy families

We compare three families of decentralized strategies that differ in their underlying correlation resources.

a. Independent classical sampling. Each agent samples \tilde{a}_i independently and uniformly from \mathcal{A} . This provides a baseline with no shared correlation resource where the joint distribution factorizes. All strategy families considered here are permutation-invariant (agents use identical local response rules), so the resulting marginals $P(a_i)$ are identical across agents. Accordingly, the relevant “independent baseline” is the product distribution $\prod_{i=1}^N P(a_i)$ with this common marginal. When reporting that a strategy lies “below the independent baseline” at a given (p, λ) , we evaluate this product baseline pointwise using the empirical marginal estimated at that same (p, λ) . All strategy families considered here are permutation-invariant (agents use identical local response rules), so the resulting marginals $P(a_i)$ are identical across agents. Accordingly, the relevant “independent baseline” is the product distribution $\prod_{i=1}^N P(a_i)$ with this common marginal.

b. Shared-latent classical coordination. Agents share a classical latent variable $L \in \mathcal{A}$. Conditioned on L , each agent outputs L with probability q and samples uniformly from \mathcal{A} with probability $1 - q$. The parameter q controls the strength of classical shared randomness. This family is the explicit *restricted* symmetric classical baseline used throughout this work: the shared latent takes values in the same action alphabet and each agent uses the same conditional response $P(\tilde{a}_i | L)$. More general classical shared-randomness constructions (e.g., shared variables encoding role assignments or permutations) are outside the scope of this baseline. As $q \rightarrow 1$, this strategy converges to the “copy” limit ($a_1 = \dots = a_N$), maximizing total correlation within this baseline family but also maximizing collision probability.

c. Quantum-correlated coordination. Agents share an N -partite entangled W state prior to the round:

$$|W_N\rangle = \frac{1}{\sqrt{N}} \sum_{k=1}^N |0 \dots 1_k \dots 0\rangle, \quad (1)$$

chosen for its robustness to local noise and particle loss in distributed settings [32, 33, 39].

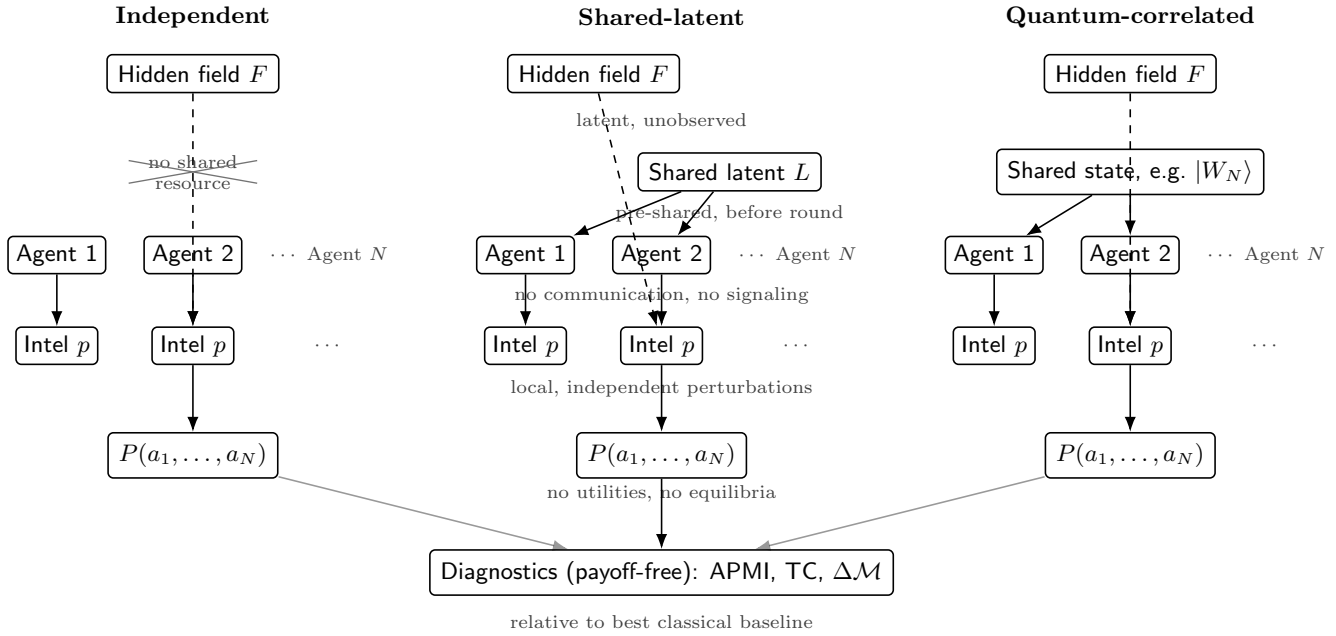


FIG. 1. Schematic of the Hidden-Field Coordination (HFC) model and strategy families. Each round samples a latent hidden field F that remains unobserved by agents and influences only the local intel perturbations (rate p). Agents act without communication; correlation arises solely from a pre-shared resource established prior to the round. We compare independent sampling, classical shared-latent coordination (shared variable L), and quantum-correlated coordination (shared state (e.g. $|W_N\rangle$)). The analyzed object is the empirical joint-action distribution $P(a_1, \dots, a_N)$, from which payoff-free diagnostics (APMI, total correlation TC, and differentials $\Delta\mathcal{M}$ relative to the best classical baseline) are computed.

To strictly enforce the no-communication constraint, agents utilize a *Spontaneous Leader Election* protocol based solely on local projective measurements in the computational basis ($b_i \in \{0, 1\}$). If an agent measures $b_i = 1$, they assume the role of “Leader” and target action 1. If they measure $b_i = 0$, they assume the role of “Follower” and sample uniformly from the remaining targets $\{2, \dots, M\}$. This rule is local, symmetric, and accounts for the physical reality of noise (e.g., multiple or zero excitations) without assuming global knowledge of other agents’ outcomes.

C. Information-theoretic observables

To characterize coordination independently of outcomes, we analyze $P(\mathbf{a})$ using:

a. Average pairwise mutual information (APMI):

$$\text{APMI} = \frac{2}{N(N-1)} \sum_{i < j} I(a_i; a_j), \quad (2)$$

summarizing pairwise structure across the team [12].

b. Total correlation (TC):

$$\text{TC}(\mathbf{a}) = \sum_{i=1}^N H(a_i) - H(\mathbf{a}), \quad (3)$$

which captures genuinely multipartite dependence [13]. TC vanishes if and only if the joint distribution factorizes.

D. Differential classical baselines

We also quantify collisions via the *average pairwise coincidence*

$$\text{Coin} = \frac{2}{N(N-1)} \sum_{i < j} \Pr[a_i = a_j]. \quad (4)$$

For completeness, one may also define the *global* collision probability $\Pr[a_1 = \dots = a_N]$; throughout this paper, the term “collision” refers to the pairwise coincidence functional Coin unless explicitly stated otherwise. For completeness, one may also define the *global* collision probability $\Pr[a_1 = \dots = a_N]$; throughout this paper, the term “collision” refers to the pairwise coincidence functional Coin unless explicitly stated otherwise.

We report observables relative to the strongest classical baseline within the shared-latent family:

$$\Delta\mathcal{M} = \mathcal{M}_{\text{quant}} - \max \left\{ \mathcal{M}_{\text{ind}}, \max_{q \in [0,1]} \mathcal{M}_{\text{shared}}(q) \right\}. \quad (5)$$

Within this restricted symmetric baseline, increasing \mathcal{M} is typically achieved by increasing action-alignment

(copying), so *negative* differentials quantify separation between the alignment-based classical optimum (over q) and the collision-suppressing quantum structure. This allows us to study quantum correlations as *distributional objects*, disentangled from payoff optimization or signaling.

III. RESULTS

We report how entanglement-mediated sampling in the Hidden-Field Coordination (HFC) model modifies the *distributional structure* of multi-agent coordination. Throughout, we compare three strategy families: (i) independent classical sampling, (ii) a shared-latent classical coordination model (optimized over q for differential metrics), and (iii) a quantum-correlated strategy implemented by mapping measurement outcomes of an N -qubit W state to local actions via the *Spontaneous Leader Election* protocol. All strategies are evaluated under identical hidden-field realizations and identical local intel perturbations; the quantum strategy additionally includes depolarizing noise of strength λ applied prior to measurement. Rather than framing outcomes in terms of payoff optimization, we focus on observable signatures in the joint action distributions that distinguish coordination mechanisms under identical no-communication constraints and identical hidden-field/intel channels.

A. Joint-action signatures

We visualize representative low-dimensional marginals to illustrate qualitative coordination signatures. Figure 2 shows empirical two-agent joint-action distributions. The shared-latent classical strategy (middle panels) concentrates probability along the diagonal ($a_i = a_j$), reflecting correlations dominated by action equality (copying). Within the restricted shared-latent baseline family defined in Sec. II, increasing dependence proceeds primarily through this alignment mechanism.

In contrast, the quantum strategy (right panels) exhibits a distinct collision-suppressing geometry. High probability mass is concentrated in off-diagonal configurations where exactly one agent assumes the Leader role ($a = 1$). This structure demonstrates how the W state's spontaneous symmetry breaking allows agents to coordinate on unequal roles without pre-assigned indices. Crucially, the quantum map shows a "hole" at the $(1, 1)$ coordinate compared to the classical case, demonstrating (within the specified model and baseline family) that entanglement-mediated sampling can coordinate roles while suppressing collisions on the Primary action.

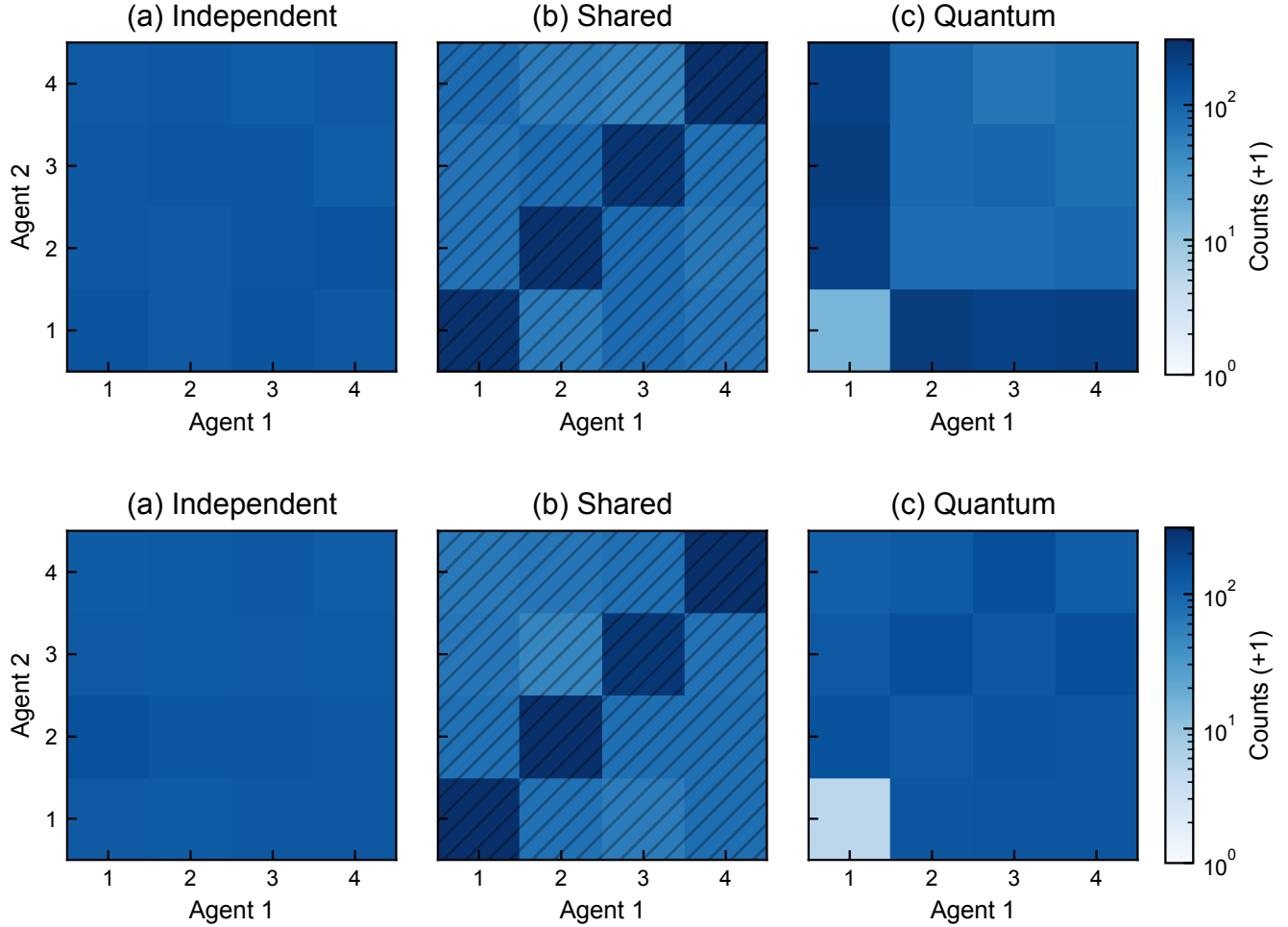


FIG. 2. Representative joint-action maps for team sizes $N = 3$ (top) and $N = 5$ (bottom). The shared-latent model (middle panels, diagonal strips, $q = 0.7$) shows concentration along the $a_1 = a_2$ diagonal, indicating coordination achieved through action alignment (copying). In contrast, the quantum strategy (right panels) displays an “L-shaped” relational structure. Probabilities are concentrated where one agent is the Leader ($a = 1$) and others are Followers ($a \neq 1$), effectively distributing probability mass away from the collision point at $(1, 1)$.

B. Coordination geometry in the (APMI, Coincidence) plane

We project each strategy into a two-dimensional plane spanned by average pairwise coincidence (Coin) and average pairwise mutual information (APMI). Figure 3 shows coordination “trails” as the intel rate p is varied. The shared-latent classical strategy moves toward the top-right corner, demonstrating that increasing coordination (APMI) in classical systems necessitates increasing action identity (collisions).

By contrast, the quantum strategy occupies a distinct region in the bottom-left, often dipping *below* the coincidence level of independent agents. Within the classical baseline family, reducing coincidence requires weakening the shared-latent component, which drives APMI toward zero. The entanglement-mediated mapping, however, maintains nontrivial dependence while occupying a lower-coincidence region. This separation is a robust geometric feature of the W -state resource that persists as N increases, representing a departure from the alignment-based dependence of the restricted shared-latent classical baseline family studied here.

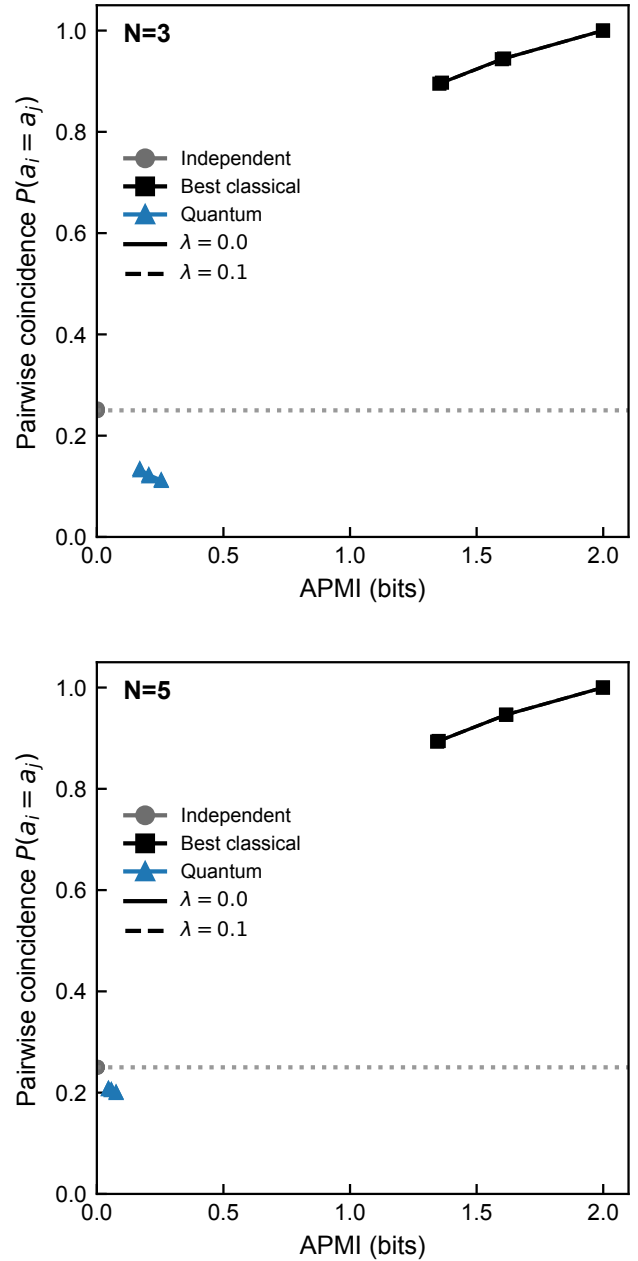


FIG. 3. Coordination geometry trails for $N = 3$ (top) and $N = 5$ (bottom). The shared-latent classical model (black squares) traces a path toward high coincidence, confirming that the restricted shared-latent classical baseline increases correlation (APMI) primarily through alignment. The quantum strategy (blue triangles) occupies a distinct region characterized by stable APMI but low coincidence, sitting below the independent baseline (grey dashed line). This reveals a geometric separation relative to the restricted shared-latent classical baseline: entanglement circumvents the trade-off between coordination and collision risk within that baseline family.

C. Global dependence across intel rate and depolarizing noise

Pairwise metrics often obscure genuinely multipartite structure. To capture global dependence, we compute the total correlation (TC). We compare strategies using the differential $\Delta\text{TC}(p, \lambda)$ relative to the best-performing classical baseline.

Figure 4 reports ΔTC for $N = 3$ and $N = 5$. Across the explored parameter region, ΔTC remains negative. This negative differential provides a critical information-theoretic insight: classical strategies maximize total correlation by converging to the “copy” limit ($a_1 = \dots = a_N$). While this yields a higher raw magnitude of shared bits, it results in maximal local collisions. The quantum strategy sacrifices raw magnitude—paying a “bit-cost”—to achieve its collision-suppressing structure. Thus, $\Delta\text{TC} < 0$ is not a failure of quantum coordination, but a signature of its efficiency in maintaining global dependence without resorting to redundant alignment.

Similarly, Fig. 5 shows the differential in APMI, which also remains negative. This reinforces the conclusion that the value of the quantum resource lies in its *geometry* (the avoidance of collisions seen in Figure 3) rather than its absolute information-theoretic magnitude.

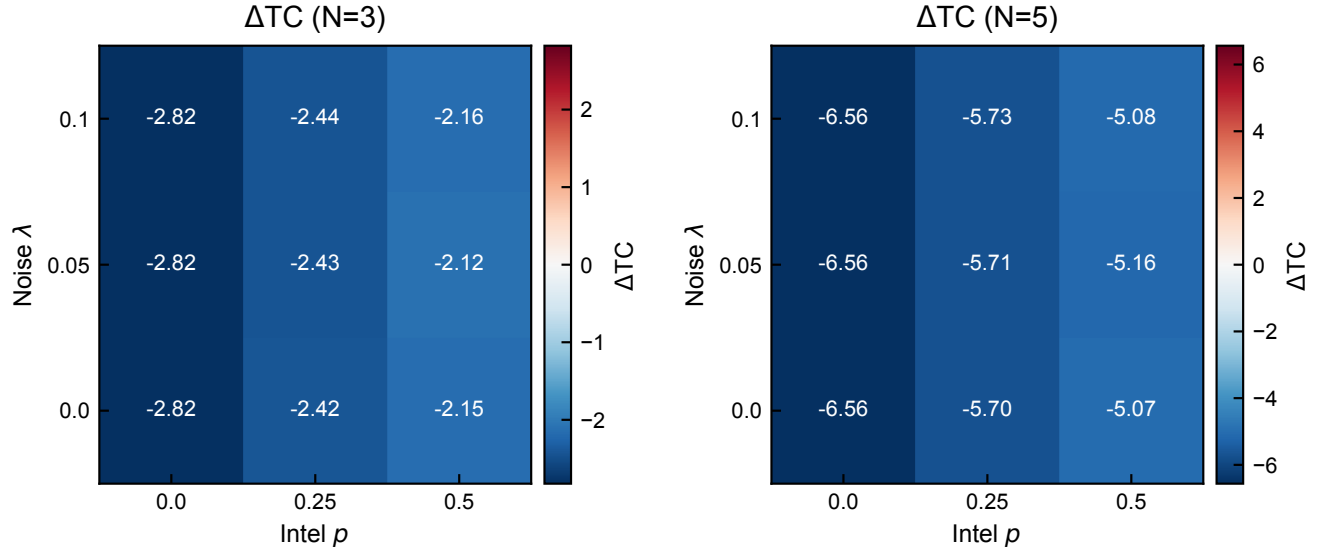


FIG. 4. Differential Total Correlation ΔTC for $N = 3$ and $N = 5$. Consistently negative values across the noise (λ) and intel (p) sweep confirm that the classical baseline achieves higher raw dependence via alignment. The quantum strategy utilizes the W state to generate relational correlations, sacrificing total shared information to remain in a low-collision regime.

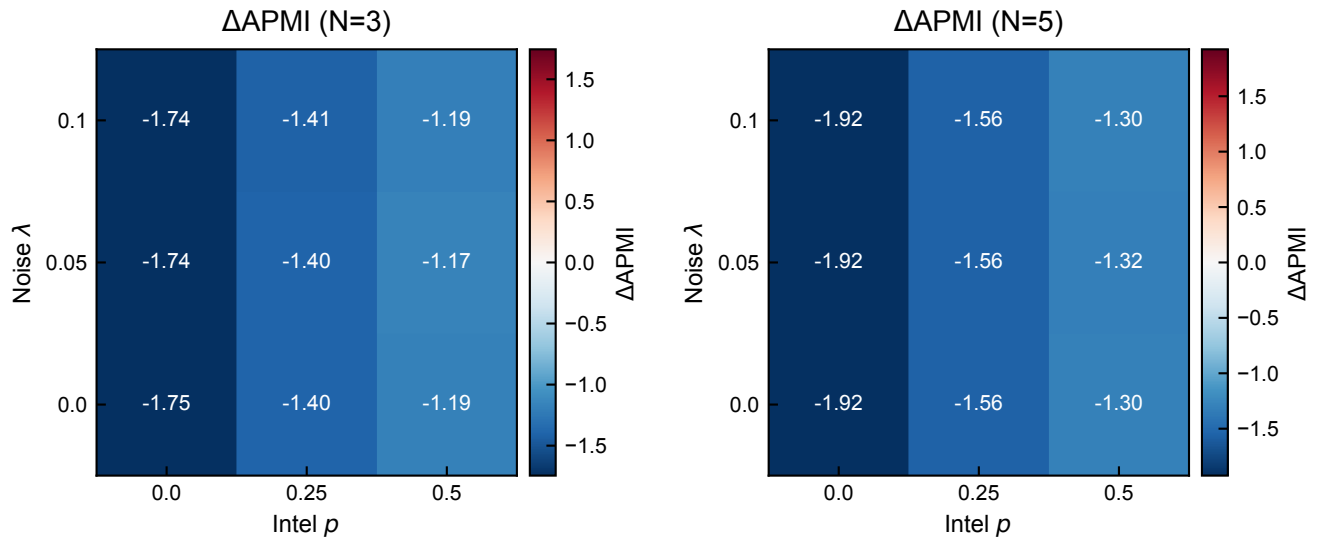


FIG. 5. Pairwise-structure differential ΔAPMI between the quantum strategy and the best classical baseline across intel rate p and depolarizing strength λ , shown for $N = 3$ (left) and $N = 5$ (right). Here $\Delta\text{APMI} = \text{APMI}_{\text{quant}} - \max(\text{APMI}_{\text{ind}}, \max_{q \in [0,1]} \text{APMI}_{\text{shared}}(q))$ evaluated *locally at each* (p, λ) . The consistently negative or near-zero differentials highlight that the quantum strategy does not aim to maximize raw information-theoretic magnitude. Instead, its primary advantage lies in the *geometric distribution* of those correlations (lower coincidence) relative to the classical baseline, which is forced into action-alignment to achieve comparable APMI levels.

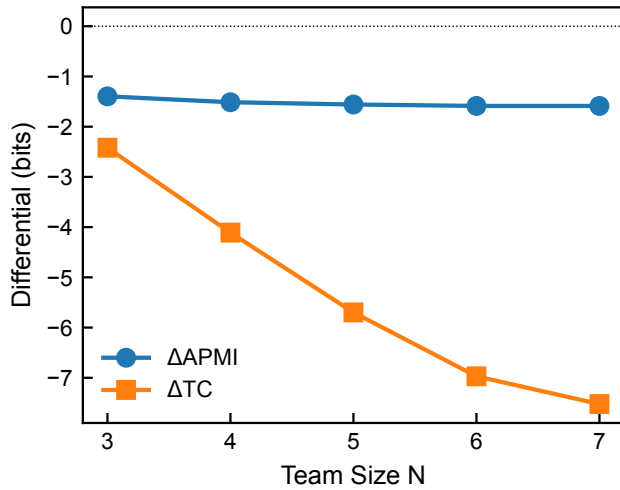


FIG. 6. Scaling of correlation differentials at $(p = 0.25, \lambda = 0)$ for $N \in \{3, 4, 5, 6, 7\}$. Over the tested range, $\Delta\text{TC}(N)$ becomes increasingly negative while $\Delta\text{APMI}(N)$ remains comparatively stable, indicating that the separation between the quantum strategy and the best-performing classical baseline within the restricted shared-latent family is more pronounced in a global dependence metric than in a pairwise one.

D. Scaling of geometric separation

We examine how these signatures vary with team size at a fixed operating point ($p = 0.25, \lambda = 0$) by extending the analysis to $N \in \{3, 4, 5, 6, 7\}$. Figure 6 plots the differentials $\Delta\text{APMI}(N)$ and $\Delta\text{TC}(N)$.

Over the tested range, we observe a systematic trend: $\Delta\text{TC}(N)$ becomes increasingly negative as N grows, while $\Delta\text{APMI}(N)$ remains comparatively stable. This indicates that the gap in raw information-theoretic magnitude between the quantum strategy and the best-performing classical baseline within the restricted shared-latent family grows more strongly in a global metric (TC) than in a pairwise one (APMI). Together with the coincidence diagnostics, this behavior is consistent with a structural distinction that is primarily multipartite: the quantum strategy maintains a non-alignment-based relational profile under the fixed local mapping, whereas the restricted shared-latent baseline can increase dependence primarily by shifting probability mass toward action alignment.

IV. METHODS

A. Hidden-Field Coordination model

We study a Hidden-Field Coordination (HFC) task involving N agents and M discrete action targets. At the beginning of each round, an external hidden field selects a subset $F \subset \{1, \dots, M\}$ of cardinality K . This as-

signment is random, exogenous, and unobserved by the agents. The hidden field does not constitute a player and does not respond to agent actions.

Each agent i produces an initial target proposal $\tilde{a}_i \in \{1, \dots, M\}$ according to a strategy-dependent sampling rule. The final executed action a_i may differ from \tilde{a}_i due to a local intel perturbation process defined below.

Agents do not communicate and have no access to the hidden-field realization. All strategies are evaluated under identical hidden-field sequences and intel realizations to ensure controlled comparisons; the quantum strategy additionally includes depolarizing noise of strength λ applied prior to measurement.

B. Intel perturbation channel

Partial interaction with the hidden field is modeled as a local, agent-wise stochastic channel applied after each strategy produces an initial proposal $\tilde{a}_i \in \{1, \dots, M\}$. Each round samples a hidden field as an indicator vector $f \in \{0, 1\}^M$ with exactly K defended targets, i.e., $\sum_{t=1}^M f_t = K$. The field is unobserved by agents and fixed throughout the round.

The intel channel acts independently on each agent i and depends only on (\tilde{a}_i, f) . With probability p (the intel rate), agent i performs an “inspection”: it draws an index $T \sim \text{Unif}\{1, \dots, M\}$ and observes a noisy defended-bit

$$\hat{f}_T = f_T \oplus B, \quad B \sim \text{Bernoulli}(\epsilon), \quad (6)$$

where \oplus denotes XOR and ϵ is the intel-flip probability. If the inspected target coincides with the agent’s proposal and the noisy bit indicates “defended,”

$$\tilde{a}_i = T \text{ and } \hat{f}_T = 1, \quad (7)$$

then with probability v (the veto probability) the agent redirects its action uniformly to one of the remaining $M - 1$ targets. Thus v controls the conditional probability of redirection given that inspection is performed, the inspected index matches the proposal, and the noisy defended-bit reports “defended.”

$$a_i \sim \text{Unif}(\{1, \dots, M\} \setminus \{T\}). \quad (8)$$

In all other cases (no inspection, or inspection that does not trigger a veto), the executed action remains unchanged, $a_i = \tilde{a}_i$.

The intel channel is memoryless across rounds and conditionally independent across agents given the hidden field, and it introduces no signaling or shared randomness between agents.

C. Strategy Families

We compare three families of decentralized strategies that differ in their underlying correlation resources.

a. *Independent classical sampling.* Each agent samples \tilde{a}_i independently and uniformly from \mathcal{A} . This provides a baseline with no shared correlation resource where the joint distribution factorizes.

b. *Shared-latent classical coordination.* Agents share a classical latent variable $L \in \mathcal{A}$. Conditioned on L , each agent outputs L with probability q and samples uniformly from \mathcal{A} with probability $1 - q$. This one-parameter family is the restricted symmetric classical baseline used throughout the paper (the shared latent takes values in the action alphabet and all agents use the same conditional response). As $q \rightarrow 1$, this strategy converges to the “copy” limit ($a_1 = \dots = a_N$), maximizing total correlation within this baseline family but also maximizing collision probability.

c. *Quantum-correlated coordination.* Agents share an N -partite entangled W state prior to the round:

$$|W_N\rangle = \frac{1}{\sqrt{N}} \sum_{k=1}^N |0 \dots 1_k \dots 0\rangle, \quad (9)$$

chosen for its robustness to local noise and particle loss [33, 39]. To ensure decentralized coordination without signaling, agents utilize a *Relational Role Mapping* protocol. Each agent i performs a local projective measurement in the computational basis ($b_i \in \{0, 1\}$). If $b_i = 1$ (excitation), the agent adopts a “Primary” role and targets action 1. If $b_i = 0$ (ground), the agent adopts a “Secondary” role and samples an action uniformly at random from the set $\{2, \dots, M\}$. This mapping is strictly local and index-equivariant; no global information regarding the total number of excitations is used by the agents.

D. Noise and Protocol Robustness

In the quantum strategy, we model decoherence via independent single-qubit depolarizing noise (λ) applied prior to measurement. The Relational Role Mapping defined in Section IV C is specifically designed to enforce the no-communication constraint under these NISQ-era conditions [36].

Under ideal conditions, the W state ensures exactly one agent measures $b_i = 1$, resulting in a perfectly coordinated occupation of the Primary role. However, if decoherence or gate errors result in multiple excitations ($\sum b_i > 1$) or none at all ($\sum b_i = 0$), the agents cannot “re-negotiate” or communicate to resolve the discrepancy. They may unintentionally collide on the Primary action or leave it unoccupied. This strict adherence to local measurement outcomes ensures that no hidden communication channels are present, providing a meticulous benchmark for comparison against classical decentralized baselines.

E. Simulation procedure

Simulations are performed using the `Qiskit Aer` [40] backend. For each configuration (N, p, λ) , we generate $R = 2000$ independent rounds per replicate and average over 8 statistically independent replicates. Hidden-field realizations, intel perturbations, and quantum transpilation seeds are derived deterministically from hashed configuration identifiers. All reported observables are computed from the aggregated joint action arrays $\mathbf{a} = (a_1, \dots, a_N)$.

F. Information-theoretic metrics

a. *Average pairwise mutual information (APMI).* For each unordered agent pair (i, j) , we compute the mutual information $I(a_i; a_j)$. The APMI is the average over all pairs:

$$\text{APMI} = \frac{2}{N(N-1)} \sum_{i < j} I(a_i; a_j). \quad (10)$$

b. *Total correlation (TC).* Multipartite dependence is captured by the total correlation:

$$\text{TC}(\mathbf{a}) = \sum_{i=1}^N H(a_i) - H(\mathbf{a}), \quad (11)$$

where H denotes Shannon entropy. TC quantifies the total amount of information shared across the team.

G. Differential baselines and Interpretation

We report differential metrics relative to the strongest classical baseline (optimized over q) at each point:

$$\Delta \mathcal{M} = \mathcal{M}_{\text{quant}} - \max \left\{ \mathcal{M}_{\text{ind}}, \max_{q \in [0,1]} \mathcal{M}_{\text{shared}}(q) \right\}. \quad (12)$$

In our model, a negative ΔTC or ΔAPMI indicates that agents in the restricted shared-latent classical baseline can achieve a higher raw correlation magnitude (after optimizing q). This occurs because this baseline family increases dependence primarily by converging toward action-alignment ($a_i = a_j$), creating a “copy-cat” distribution. In contrast, the quantum strategy utilizes its shared entanglement to maintain a distinct coordination regime that suppresses collisions. Thus, the value of the quantum strategy is not found in the magnitude of shared bits, but in the geometric separation of those bits away from the high-collision diagonal of the joint-action space.

H. Reproducibility

All figures are generated using a deterministic pipeline. Random seeds for noise and intel perturbations are fixed.

The simulation and plotting scripts reproduce all numerical values and trends shown in the main text.

V. DISCUSSION

The Hidden-Field Coordination (HFC) model introduced in this work was designed to isolate correlation structure in decentralized multi-agent systems independently of payoff optimization, equilibrium selection, or communication. Within this controlled setting, our results demonstrate a qualitative geometric distinction between classical alignment-based strategies and entanglement-mediated coordination.

A central observation is the robust separation between the “alignment” regime of classical coordination and the “relational” regime of quantum coordination. As shown in the geometric trails (Fig. 3), the shared-latent classical baseline maximizes correlation only by driving the system toward high action coincidence (the diagonal). This creates a fundamental classical trade-off: agents can be highly correlated (by copying) or collision-suppressing (by randomizing), but not both. The quantum strategy, utilizing the W state, breaks this trade-off dynamically. It preserves rule symmetry (all agents follow the same conditional logic) while allowing the state itself to spontaneously break symmetry round-by-round. This enables significant global dependence (as evidenced by nonzero Total Correlation in the noiseless limit) while reducing local collisions relative to the classical alignment baseline.

The negative differential total correlation (ΔTC) observed in Fig. 4 quantifies this separation. It confirms that classical common-cause models achieve higher raw dependence, but only by paying the cost of maximal collision probability. The quantum strategy sacrifices raw bit-count relative to this “copying maximum” to access a collision-suppressing geometry that is inaccessible to the restricted shared-latent symmetric classical baseline family studied here.

The choice of W states as the primary resource is motivated by their unique structure for decentralized tasks. Unlike GHZ-type states, which concentrate correlations into global phases that are highly fragile to local perturbations, the W state provides a “relational index” (the excitation position k) that is naturally suited for distributing distinct, coordinated roles among agents. This allows the quantum strategy to generate nonzero total correlation while maintaining robustness to the local “intel” perturbations that would otherwise collapse more rigid entanglement structures.

Taken together, these findings support a reframing of quantum coordination in decentralized systems. Rather than viewing entanglement solely as a means to “boost” correlation magnitude, it should be viewed as a structural resource that reshapes the geometry of feasible joint-action distributions. From this perspective, the primary advantage of the quantum resource is its ability to ac-

cess a collision-suppressing coordination regime that is not achieved by the shared-latent classical baseline family considered here. The HFC framework makes this effect explicit by separating exogenous latent structure from coordination mechanisms and by evaluating correlation differentials relative to the strongest classical baselines permitted by the model. This approach complements recent efforts [41, 42] to characterize quantum correlations in networked and multi-agent settings beyond outcome-centric or equilibrium-based analyses.

Appendix A: Pairwise differential diagnostic

Figure 5 reports the pairwise differential $\Delta APMI(p, \lambda)$ for $N = 3$ and $N = 5$. Across the explored (p, λ) grid, the pairwise differential is comparatively small in magnitude and remains negative in regions where the quantum strategy exhibits distinct geometric structure. This behavior indicates that the dominant structural distinction between the coordination strategies is not captured by changes in two-agent marginals alone. Instead, the quantum strategy primarily redistributes dependence into higher-order correlations that preserve the relational structure of the team without enforcing the pairwise alignment (and consequent collisions) inherent to the classical common-cause baseline.

Appendix B: Shared-latent quality scan

To characterize the classical correlation-collision trade-off explicitly, we perform a scan over the shared-latent coordination strength q . For each configuration (N, p, λ) , the total correlation of the shared-latent classical model, $TC_{\text{shared}}(q)$, is evaluated across $q \in [0, 1]$ and compared against the independent baseline and the quantum strategy.

Figure 7 plots $TC_{\text{shared}}(q)$ (mean and standard deviation) together with horizontal references for TC_{ind} and TC_{quant} . As q increases, the shared-latent model interpolates between independent sampling and strong action-equality correlations, producing a monotonic increase in total correlation. Crucially, the classical curve eventually exceeds the quantum reference level (dashed line) in the high- q regime.

However, this crossover occurs precisely where the classical strategy converges toward the “copy” limit ($a_i = a_j$), maximizing collision probability. The quantum strategy achieves its stable total correlation level *without* requiring the high coordination strength q associated with action collisions. This scan confirms that the negative differentials reported in the main text are not artifacts of suboptimal classical parameters, but rather reflect a fundamental geometric separation within the restricted shared-latent baseline family studied here: the shared-latent classical baseline maximizes correlation via

alignment, while the quantum strategy maintains dependence via anti-coordination.

Appendix C: Convergence and stability

To verify that the reported information-theoretic metrics are not artifacts of finite sampling, we examine their convergence as a function of simulated rounds. Figure 8 shows the evolution of the estimated global differential ΔTC for representative configurations.

The estimates stabilize at their negative values well before the maximum number of rounds used in the main analysis. This behavior confirms that the reported separation between classical and quantum correlation structures is a robust feature of the underlying probability distributions rather than statistical noise.

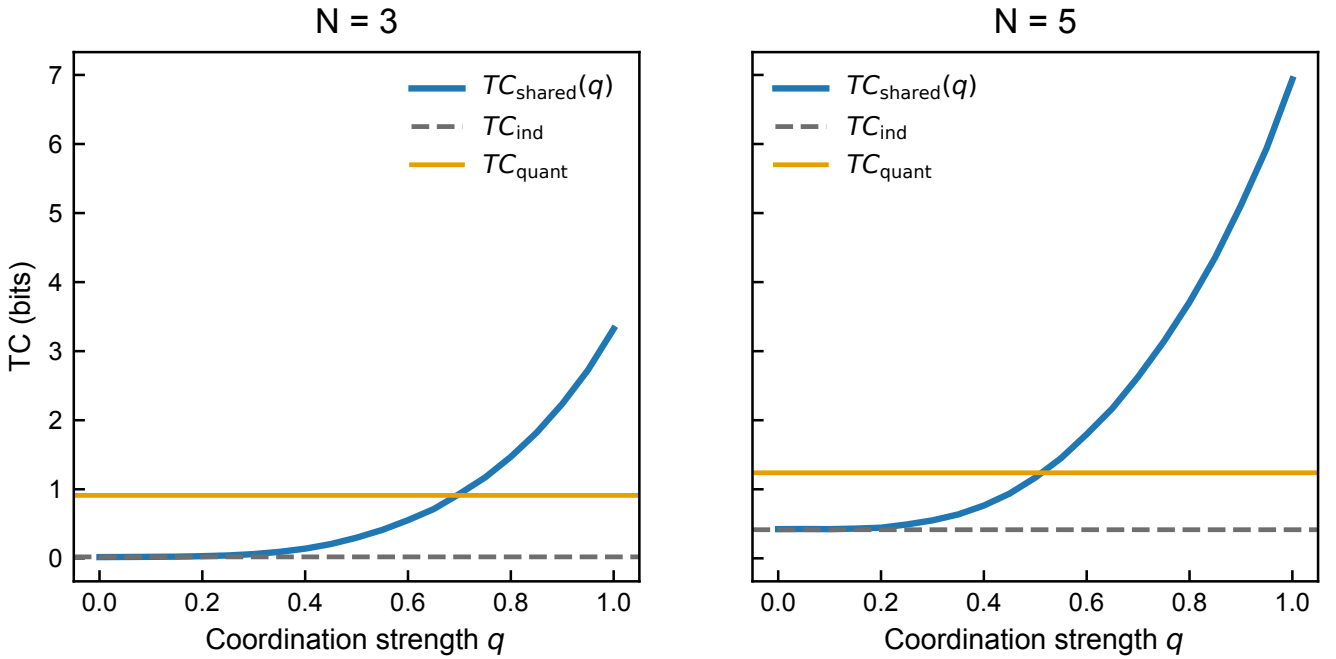


FIG. 7. Shared-latent quality scan for Total Correlation (TC). The classical shared-latent strategy (blue curve) monotonically increases TC as the coordination strength q grows. The orange line marks the TC level achieved by the quantum strategy. Crucially, the classical strategy only surpasses the quantum benchmark in the high- q regime ($q \gtrsim 0.65$ for $N = 3$; $q \gtrsim 0.50$ for $N = 5$), which corresponds to the region of high action alignment and collisions. This confirms that the quantum strategy achieves a significant tier of correlation magnitude "for free" (without enforcing alignment), whereas classical strategies must explicitly enforce copying to reach comparable levels.

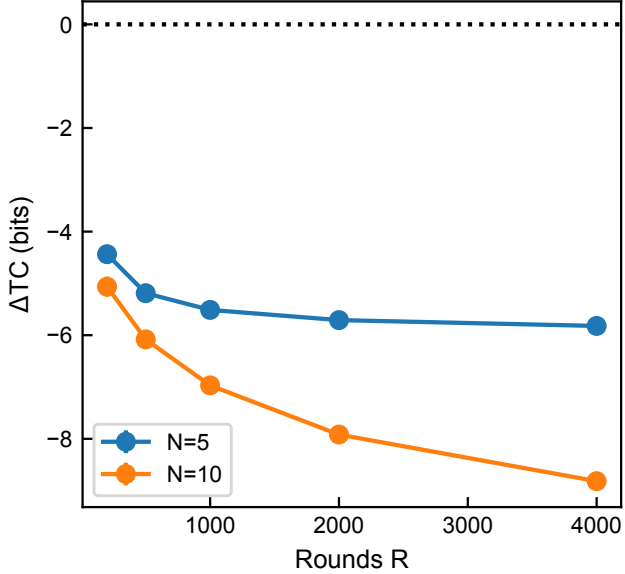


FIG. 8. Convergence of the global differential ΔTC as a function of simulation rounds R . The differential stabilizes at a distinct negative value for $R \geq 2000$, confirming that the measured separation is a robust feature of the underlying probability distributions and not an artifact of finite sampling noise. Data shown for $N = 5$ and $N = 10$ at fixed parameters ($p = 0.25, \lambda = 0$).

[1] J. S. Bell, On the Einstein Podolsky Rosen paradox, *Physics Physique Fizika* **1**, 195 (1964).

[2] J. F. Clauser, M. A. Horne, A. Shimony, and R. A. Holt, Proposed experiment to test local hidden-variable theories, *Phys. Rev. Lett.* **23**, 880 (1969).

[3] N. Brunner, D. Cavalcanti, S. Pironio, V. Scarani, and S. Wehner, Bell nonlocality, *Rev. Mod. Phys.* **86**, 419 (2014).

[4] T. Fritz, Beyond bell's theorem: correlation scenarios, *New Journal of Physics* **14**, 103001 (2012).

[5] M. Navascués, S. Singh, and A. Acín, Connector tensor networks: a renormalization-type approach to quantum certification, *Physical Review X* **10**, 021064 (2020).

[6] D. Rosset, C. Branciard, T. J. Barnea, G. Pütz, N. Brunner, and N. Gisin, Nonlinear bell inequalities tailored for quantum networks, *Phys. Rev. Lett.* **116**, 010403 (2016).

[7] A. Acín and L. Masanes, Certified randomness in quantum physics, *Nature* **540**, 213 (2016).

[8] E. Wolfe, R. W. Spekkens, and T. Fritz, The inflation technique for causal inference with latent variables, *Journal of Causal Inference* **7**, 20170020 (2019).

[9] J. Pearl, *Causality* (Cambridge university press, 2009).

[10] A. Tavakoli, A. Pozas-Kerstjens, M.-X. Luo, and M.-O. Renou, Bell nonlocality in networks, *Reports on Progress in Physics* **85**, 056001 (2022).

[11] C. E. Shannon, A mathematical theory of communication, *The Bell System Technical Journal* **27**, 379 (1948).

[12] T. M. Cover and J. A. Thomas, *Elements of Information Theory* (Wiley-Interscience, 2006).

[13] S. Watanabe, Information theoretical analysis of multivariate correlation, *IBM Journal of Research and Development* **4**, 66 (1960).

[14] Z. Walczak, Total correlations and mutual information, *Physics Letters A* **373**, 1818 (2009).

[15] R. A. A. Ince, Measuring multivariate information flow, *Entropy* **19**, 318 (2017).

[16] S.-i. Amari, *Information Geometry and Its Applications* (Springer, 2016).

[17] N. Ay and D. Polani, Information flows in causal networks, *Advances in complex systems* **11**, 17 (2008).

[18] P. Cuff, H. Permuter, and T. Cover, Coordination capacity, *IEEE Transactions on Information Theory* **56**, 4181 (2010).

[19] J. Eisert, M. Wilkens, and M. Lewenstein, Quantum games and quantum strategies, *Phys. Rev. Lett.* **83**, 3077 (1999).

[20] A. C. Maioli, M. H. M. Passos, W. F. Balthazar, M. de Oliveira, M. F. Santos, and P. L. Saldanha, Quantization and experimental realization of the colonel blotto game, *Quantum Information Processing* **18**, 10 (2019).

[21] V. N. Kolokoltsov, Dynamic quantum games, *Dynamic Games and Applications* **12**, 552 (2022).

[22] S. Bugu, F. Ozaydin, and T. Kodera, Surpassing the classical limit in magic square game with distant quantum dots coupled to optical cavities, *Scientific Reports* **10**, 22202 (2020).

[23] S. Bugu, Entanglement as a strategic resource in adversarial quantum games, *arXiv preprint arXiv:2510.22444* (2025).

[24] H. Natur and U. Pereg, Quantum coordination rates in multi-user networks, *IEEE Transactions on Information Theory* **71**, 4428 (2025).

[25] S. K. Özdemir, E. Matsunaga, T. Tashima, T. Yamamoto, M. Koashi, and N. Imoto, An optical fusion gate for W states, *New Journal of Physics* **13**, 103003 (2011).

[26] S. Bugu, C. Yesilyurt, and F. Ozaydin, Enhancing the W-state quantum-network-fusion process with a single Fredkin gate, *Phys. Rev. A* **87**, 032331 (2013).

[27] F. Ozaydin, S. Bugu, C. Yesilyurt, A. A. Altintas, M. Tame, and S. K. Özdemir, Fusing multiple W states simultaneously with a Fredkin gate, *Phys. Rev. A* **89**, 042311 (2014).

[28] B. Thapa, O. Moran, D.-K. Vu, and F. Ozaydin, Expanding a 4-qubit dicke state to a 5-qubit dicke state with limited qubit access, *Quantum Information Processing* **24**, 401 (2025).

[29] R. Horodecki, P. Horodecki, M. Horodecki, and K. Horodecki, Quantum entanglement, *Reviews of Modern Physics* **81**, 865 (2009).

[30] O. Gühne and G. Tóth, Entanglement detection, *Physics Reports* **474**, 1 (2009).

[31] M. Ma, Y. Li, and J. Shang, Multipartite entanglement measures: A review, *Fundamental Research* **5**, 2489 (2025).

[32] W. Dür, G. Vidal, and J. I. Cirac, Three qubits can be entangled in two inequivalent ways, *Phys. Rev. A* **62**, 062314 (2000).

[33] L.-H. Zhu, Z. Zhu, G.-L. Lv, C.-Q. Ye, and X.-Y. Chen, Robustness of entanglement for Dicke-W and Greenberger-Horne-Zeilinger mixed states, *Entropy* **26**, 804 (2024).

[34] M. Huber, F. Mintert, A. Gabriel, and B. C. Hiesmayr, Detection of high-dimensional genuine multipartite entanglement of mixed states, *Physical Review Letters* **104**, 210501 (2010).

[35] M. A. Nielsen and I. L. Chuang, *Quantum Computation and Quantum Information* (Cambridge University Press, 2010).

[36] J. Preskill, Quantum computing in the nisq era and beyond, *Quantum* **2**, 79 (2018).

[37] F. G. S. L. Brandão and A. W. Harrow, Quantum de finetti theorems under local measurements with applications, *Communications in Mathematical Physics* **353**, 469 (2017).

[38] A. W. Harrow and A. Montanaro, Quantum computational supremacy, *Nature* **549**, 203 (2017).

[39] R. Chaves and L. Davidovich, Robustness of entanglement as a resource, *Phys. Rev. A* **82**, 052308 (2010).

[40] A. Cross, The ibm q experience and qiskit open-source quantum computing software, in *APS March meeting abstracts*, Vol. 2018 (2018) pp. L58–003.

[41] W.-T. Kao, C.-Y. Huang, T.-J. Tsai, S.-H. Chen, S.-Y. Sun, Y.-C. Li, T.-L. Liao, C.-S. Chuu, H. Lu, and C.-M. Li, Scalable determination of multipartite entanglement in quantum networks, *npj Quantum Information* **10**, 73 (2024).

[42] P. M. Poggi and M. H. Muñoz-Arias, Measurement-induced multipartite-entanglement regimes in collective spin systems, *Quantum* **8**, 1229 (2024).